

接地导体机电阻抗均匀腐蚀评估技术*

黄宴委, 陈耀捷, 张皓骏, 方舟

(福州大学自动化系 福州, 350116)

摘要 针对传统检测方法难以简便地检测并评估接地导线的腐蚀程度问题,提出一种基于机电阻抗技术的接地导体腐蚀程度的评估方法。首先,应用金属电化学腐蚀理论,建立接地导体的半径参数化腐蚀模型;其次,通过对系统机电阻抗以及导体机械导纳的分析,建立一种共振频率与半径参数的腐蚀模型;然后,利用有限元仿真方法激励获取接地导体共振频率与腐蚀参数信号,并采用最小二乘线性拟合获得腐蚀模型参数;最后,进行了仿真与实验。结果表明:相较于对称传感器布置方式,非对称传感器布置方式下得到的机电阻抗能够更好地反映出腐蚀参数的变化;利用有限元仿真与最小二乘法建立的线性模型能够有效预测接地导体的腐蚀参数;线性模型预测数据非常接近实验数据,表明可以利用线性模型来预测实际接地导体的腐蚀程度。

关键词 接地导体;参数化腐蚀模型;机电阻抗;有限元仿真

中图分类号 TH878

引言

接地导体的腐蚀程度关系到电网运行的安全性^[1],然而腐蚀诊断技术一直尚未有突破^[2]。常规的诊断方法有摇表法、电磁场检测法^[3]和电化学方法等,但这些方法难以直观地检测导体的腐蚀程度且容易受到工作环境的干扰,影响测量结果的准确性。

近年来,机电阻抗技术已被广泛应用于各类结构的损伤检测中^[4]。Nguyen等^[5]结合一维卷积神经网络和机电阻抗技术,自动提取损伤特征来监测钢筋混凝土梁的损伤。Zuo等^[6]利用多个压电传感器的机电阻抗识别了管道中的早期裂纹。机电阻抗技术也被应用于金属的腐蚀检测。Tamhane等^[7]利用机电阻抗技术评估了金属薄片的整体腐蚀。Ai等^[8]在钢梁上测试了压电陶瓷(piezoelectric ceramic transducer,简称PZT)与局部腐蚀的距离对整体系统机电阻抗的影响。Li等^[9]评估了在不同湿度环境下金属棒腐蚀质量与3种损伤评价指标的关系。Wang等^[10]结合机电阻抗技术设计了一种变截面圆锥杆腐蚀探针。这些研究利用损伤指标或神经网络评估了结构的损伤程度,但尚未从理论上建立机电阻抗特征与损伤的关联性^[11]。

笔者针对接地导线腐蚀程度难以评估的问题,提出一种利用机电阻抗技术评估接地导体腐蚀程度

的方法。首先,分析了金属腐蚀对接地导体形状的影响,将接地导体半径变化量 Δr 视为腐蚀参数,建立接地导体参数化腐蚀模型;其次,通过对系统机电阻抗的分析并结合接地导体机械导纳与共振频率的联系,建立非对称传感器布局机电阻抗下共振频率 f_m 与腐蚀参数 Δr 的模型,建立机电阻抗特征与腐蚀的关联模型;然后,利用有限元对 f_m 与 Δr 的信号进行数值仿真,并利用最小二乘线性拟合获得腐蚀模型参数 k_m ;最后,设计了实验平台,采用非对称传感器布置机电阻抗技术检测接地导体的腐蚀,验证了该方法具有很高的可行性与准确性。

1 金属导体腐蚀参数化模型

自然条件下,接地金属导体在土壤中一般会生电学腐蚀^[12]。金属导体电学腐蚀程度由其损失质量 m_t 来表征,即

$$m_t = MIt/zF \quad (1)$$

其中: M 为金属原子质量; I 为施加在导体上的电流; t 为通过电流的时间; z 为腐蚀生成金属阳离子对应的电荷数; $F=96\ 500$ A/S,为法拉第常数。

由于杆状接地金属导体长径之比较大,腐蚀对其长度的影响相比于对半径的影响较小。导体内部未腐蚀部分密度不发生改变,则接地导体的腐蚀质量转化为用半径减小量 Δr 来表征,即

* 国家自然科学基金资助项目(52205557);福建省自然科学基金资助项目(2023J01230170)

收稿日期:2023-11-13;修回日期:2024-12-10

$$m_i = (r_1^2 - r_2^2) \pi l \rho = (2r_1 - \Delta r) \Delta r \pi l \rho \quad (2)$$

其中： r_1 、 r_2 分别为腐蚀前后接地导体半径； l 为导体长度； ρ 为导体密度； $\Delta r = r_1 - r_2$ 。

根据式(2)可知，金属导体的腐蚀损失质量与导体半径减小量有关^[12]，具体为：①当轻度腐蚀($\Delta r \leq 0.29r_1$)时， Δr 较小，可忽略掉 $(\Delta r)^2$ ，则 $m_i \approx 2r_1 \Delta r \pi l \rho$ ；②当中度腐蚀($0.29r_1 < \Delta r < 0.68r_1$)时， $m_i = (2r_1 - \Delta r) \Delta r \pi l \rho$ ；③当严重腐蚀($\Delta r \geq 0.68r_1$)时， Δr 较大， r_2 很小，则 $m_i \approx r_1 \Delta r \pi l \rho$ 。

2 机电阻抗导体腐蚀检测技术

接地导体半径变化会改变接地导体的共振频率，本研究探索一种机电阻抗导体检测技术，分析共振频率变化量与接地导体半径变化量 Δr 之间的关系。

2.1 机电阻抗检测技术

机电阻抗检测技术利用PZT激励金属导体振动并采集金属导体的振动信号，计算阻抗变化，确定导体腐蚀程度。系统机电阻抗^[13]为

$$Z(\omega) = \left(j\omega \frac{l_p b_p}{h_p} (\epsilon_{33} - \frac{N_s(\omega)}{N_p(\omega) + N_s(\omega)} d_{31}^2 Y_{11}^E) \right)^{-1} \quad (3)$$

其中： $Z(\omega)$ 为整个系统的机电阻抗； ω 为交流电场的频率； l_p 、 b_p 、 h_p 分别为PZT的长、宽、高； ϵ_{33} 、 d_{31} 、 Y_{11}^E 分别为PZT的复介电常数、压电常数和复弹性模量； $N_s(\omega)$ 、 $N_p(\omega)$ 分别为接地导体和PZT的机械阻抗。

式(3)表明，系统机电阻抗 $Z(\omega)$ 受到PZT的机械阻抗和导体机械阻抗的影响。其中，PZT的机械阻抗 $N_p(\omega)$ 基本保持不变，因此导体机械阻抗 $N_s(\omega)$ 的改变会直接影响 $Z(\omega)$ ，可通过测量 $Z(\omega)$ 值的改变得出 $N_s(\omega)$ 的变化^[13]。系统机电阻抗 $Z(\omega)$ 可分为实部 $\text{Re}(Z(\omega))$ 与虚部 $\text{Im}(Z(\omega))$ ，其中机电阻抗实部 $\text{Re}(Z(\omega))$ 能更好地反映结构损伤^[14]，故本研究采用 $\text{Re}(Z(\omega))$ 进行分析。

2.2 金属接地导体阻抗模型

$$\begin{aligned} & \text{金属导体机械导纳} \frac{1}{N_s(\omega)} \quad [13] \text{为} \\ & \frac{1}{N_s(\omega)} = \frac{j\omega}{\rho \pi r^2} \left\{ \sum_{n=1}^{\infty} \frac{v_1^2}{(\omega_{gn}^2 - \omega^2)} + \right. \\ & \left. \frac{r}{l} \left(\frac{(2m+1)\pi}{2} \right)^2 \sum_{m=1}^{\infty} \frac{v_2^2}{(\omega_{cm}^2 - \omega^2)} \right\} \quad (4) \end{aligned}$$

其中： v_1 、 v_2 与PZT在金属导体上粘贴的位置有关； n 、 m 为对应的共振阶数； ω_{gn} 为第 n 阶纵向振动固有频率； ω_{cm} 为第 m 阶弯曲振动固有频率。

ω_{gn} 、 ω_{cm} 分别为

$$\omega_{gn} = \frac{n\pi}{l} \sqrt{\frac{E}{\rho}} \quad (5)$$

$$\omega_{cm} = \frac{1}{2} \left(\frac{(2m+1)\pi}{2l} \right)^2 \sqrt{\frac{E}{\rho}} r \quad (6)$$

其中： E 为接地导体的弹性模量。

由式(4)可知，当PZT的激励频率 ω 等于金属导体的固有频率 ω_{gn} 或 ω_{cm} 时，金属导体的机械导纳 $1/N_s(\omega)$ 达到峰值，同时机电阻抗实部 $\text{Re}(Z(\omega))$ 也达到峰值^[15]，即此时机电阻抗系统产生共振。因此，可以通过测量 $\text{Re}(Z(\omega))$ 的共振频率 ω_m 获取金属导体的固有频率，即 $\omega_m = \omega_{gn}$ 或 $\omega_m = \omega_{cm}$ ，并利用固有频率的变化来评估金属导体的腐蚀程度。

由式(5)可知，金属导体纵向振动固有频率 ω_{gn} 与腐蚀参数 Δr 无关，如果采用对称传感器布置方式，仅能产生纵向振动，其固有频率为 ω_{gn} ，通过 $\text{Re}(Z(\omega))$ 的共振频率 ω_m 只能获得 ω_{gn} 。因此，不能采用对称传感器布置方式进行腐蚀检测。

2.3 非对称传感器布置机电阻抗的腐蚀模型

由式(6)可知，金属导体 ω_{cm} 与 r 为线性关系，采用非对称传感器布置方式可激励出弯曲振动固有频率 ω_{cm} ，即

$$\begin{aligned} \Delta \omega_{cm} &= \frac{1}{2} \left(\frac{(2m+1)\pi}{2l} \right)^2 \sqrt{\frac{E}{\rho}} (r_1 - r_2) = \\ & \frac{1}{2} \left(\frac{(2m+1)\pi}{2l} \right)^2 \sqrt{\frac{E}{\rho}} \Delta r \quad (7) \end{aligned}$$

其中： $\Delta \omega_{cm} = \omega_{cm1} - \omega_{cm2}$ ，为弯曲振动固有频率偏差， ω_{cm1} 、 ω_{cm2} 分别是半径为 r_1 、 r_2 的弯曲振动固有频率。

由于 $\omega_m = \omega_{cm}$ ，结合金属导体固有频率 ω_{cm} 与机电阻抗系统 $\text{Re}(Z(\omega))$ 共振原频率 f_m 的关系，由式(7)可得到共振原频率偏移量 Δf_m 与 Δr 的关系，即

$$\begin{aligned} f_{0,m} - f_{\Delta,m} &= \Delta f_m = \\ & \left(\frac{1}{4\pi} \left(\frac{(2m+1)\pi}{2l} \right)^2 \sqrt{\frac{E}{\rho}} \right) \Delta r = k_m \Delta r \quad (8) \end{aligned}$$

其中： $f_{0,m}$ 、 $f_{\Delta,m}$ 分别为 $\Delta r = 0$ 和 $\Delta r \neq 0$ 时的导体共振频率； k_m 为模型参数。

当 m 不变时， Δf_m 与 Δr 为线性关系，且 k_m 随 m 的增大而增大。式(8)仅在金属导体长径比无穷大时

成立,因此无法由式(8)直接获得 k_m 的理论解析值。本研究利用有限元仿真技术求解 k_m 。

2.4 腐蚀模型参数求解

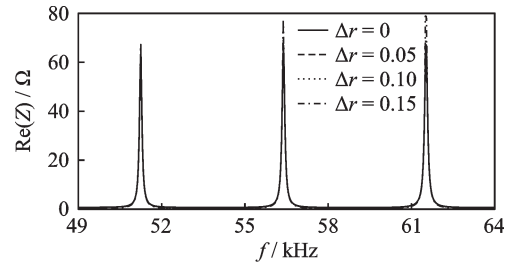
2.4.1 有限元仿真模型

在ANSYS18.0软件环境中,接地导体设置为Solid45实体体积单元,PZT设置为Solid5三维耦合场体积单元。接地导体参数如下:长度 l 为500 mm;初始半径 r_1 为4 mm;密度 ρ 为7 950 kg/m³;弹性模量 E 为 2.09×10^{11} N/m²;泊松比为0.269。PZT具体参数如下:长度 l_p 为20 mm;宽度 b_p 为5 mm;厚度 h_p 为1 mm;密度为7 500 kg/m³;压电应力系数 $e_{31} = e_{32} = -6.5$, $e_{16} = e_{25} = 17$, $e_{33} = 23.3$,单位为C/m²;相对介电常数系数 $\epsilon_{p11} = \epsilon_{p22} = 1\ 700$; $\epsilon_{p33} = 1\ 470$ 。由于接地导体与PZT的体积差异较大,接地导体采用自动扫掠网格划分,PZT采用1 mm精度网格划分。

非对称传感器布置方式是将1片PZT粘贴于接地导体的顶端,PZT长边平行于接地导体轴线,宽边与接地导体的横截面平行。对称传感器布置方式是将2片PZT对称粘贴于接地导体的顶端。将PZT正、反两面分别耦合到1个主节点上来模拟电极,对主节点施加激励电压 $U = A \sin(\omega t)$ 、正面主节点激励电压为1 V、反面主节点激励电压为0 V来模拟接地极。通过主节点的电荷量 Q 来计算电流,即 $I = j\omega \Sigma Q$ 。由于激励电压已知,利用欧姆定律计算 $Z(\omega) = U/I$,则可以获得系统机电阻抗实部 $\text{Re}(Z(\omega))$ 。测量频段为49 kHz~64 kHz,步长为30 Hz。

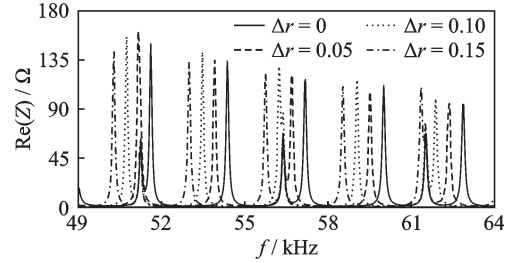
为了分析不同腐蚀参数 Δr 下的接地导体共振频率的变化,分别设置 $\Delta r = 0, 0.025, 0.05, 0.075, 0.1, 0.125, 0.15$ mm,共有7个不同 Δr 的接地导体,分别通过49 kHz~64 kHz的激励信号,得到对称传感器布置与非对称传感器布置对应的 $\text{Re}(Z(\omega))$ 。为了清晰展示导体共振频率与机电总阻抗实部的关系,分别选择 $\Delta r = 0, 0.05, 0.1$ 和0.15 mm时的机电阻抗实部与频率曲线,如图1所示。

由图1(a)可知,在对称传感器布置机电阻抗中,纵向共振频率对腐蚀参数 Δr 的变化不敏感,无法区分。由图1(b)可知:在非对称传感器布置机电阻抗中, $\Delta r = 0$ 时, $f_{0,m_0} = 51.61$ kHz, $f_{0,m_1} = 54.37$ kHz, $f_{0,m_2} = 57.19$ kHz, $f_{0,m_3} = 60.01$ kHz, $f_{0,m_4} = 62.89$ kHz; $\Delta r = 0.05$ mm时, $f_{0.05,m_0} = 51.16$ kHz, $f_{0.05,m_1} = 53.92$ kHz, $f_{0.05,m_2} = 56.68$ kHz, $f_{0.05,m_3} = 59.53$ kHz,



(a) 对称传感器布置

(a) Symmetrical sensor layout



(b) 非对称传感器布置

(b) Asymmetrical sensor layout

图1 机电阻抗实部与频率的关系

Fig.1 Relationship between impedance real part and frequency

$f_{0.05,m_4} = 62.38$ kHz; $\Delta r = 0.1$ mm时, $f_{0.1,m_0} = 50.74$ kHz, $f_{0.1,m_1} = 53.47$ kHz, $f_{0.1,m_2} = 56.26$ kHz, $f_{0.1,m_3} = 59.05$ kHz, $f_{0.1,m_4} = 61.90$ kHz; $\Delta r = 0.15$ mm时, $f_{0.15,m_0} = 50.29$ kHz, $f_{0.15,m_1} = 52.99$ kHz, $f_{0.15,m_2} = 55.75$ kHz, $f_{0.15,m_3} = 58.45$ kHz, $f_{0.15,m_4} = 61.36$ kHz。可见,当 Δr 不同时,接地导体的各阶共振频率 f_{mi} 也发生相应的变化, Δr 越大,相应的共振频率改变量 Δf_m 也越大。但是,相应腐蚀模型参数 k_m 还难以确定。

2.4.2 基于最小二乘法估计的腐蚀模型参数

由式(8)可知, k_m 值是腐蚀评估模型的关键参数。当 $\Delta r = 0, 0.025, 0.05, 0.075, 0.1, 0.125, 0.15$ mm时,由有限元仿真获得35个各阶共振频率数据,应用最小二乘法建立不同 m 值下的 f_m 与 Δr 的关系,如图2所示。图中虚线左侧为由 $\Delta r = 0, 0.025, 0.05, 0.075, 0.1, 0.125, 0.15$ mm接地导体所建立的腐蚀模型 $f_{\Delta,mi} = f_{0,mi} - k_{mi}\Delta r$ 。频率阶数为 m_i ,当 $i = 0, 1, 2, 3, 4$ 时,对共振频率偏移量 Δf_{mi} 与 Δr 进行最小二乘法线性拟合计算获得 k_{mi} , k_{mi} 分别为8.846、9.051、9.291、10.18和10.35,对应不同频率阶数下最小二乘法的估计可信度分别为0.999 6、0.998 3、0.998 4、0.996 7和0.998 1,均大于0.99。为了验证模型的准确性,分别采用5个 $\Delta r = 0.2, 0.25, 0.3, 0.35, 0.4$ mm接地导体,通过有限元仿真模型激励并测量相应 $f_{\Delta,mi}$,由式(8)计算腐蚀参数的预测值 $\Delta \hat{r}$ 。图中虚线右侧为5个 Δr 接地导体测试对比,有限元仿真激励得到的半径 Δr 与模型式(8)预测的 $\Delta \hat{r}$ 基本一致。

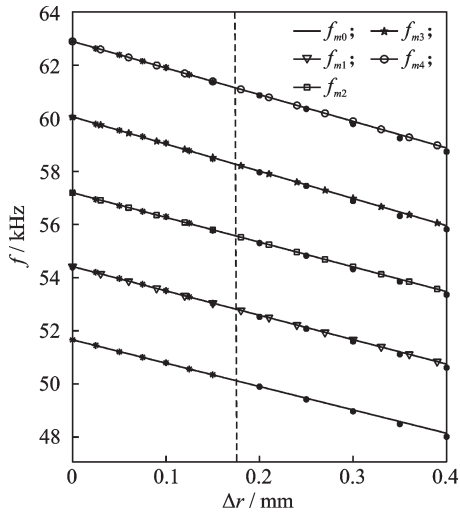


图 2 f_m 与 Δr 的关系

Fig.2 Relationship between f_m and Δr

表 1 为模型准确性分析。可见,随着 Δr 的增大,相对误差略有增大,但小于 5%。由式(8)可知, k_m 与 m 有关。共振频率偏差 Δf_m 与 Δr 的关系如图 3 所示。

表 1 模型准确性分析

Tab.1 Model accuracy analysis

$\Delta r/\text{mm}$	$\Delta \hat{r}/\text{mm}$	相对误差/%
0.20	0.203	1.5
0.25	0.254	1.6
0.30	0.307	2.3
0.35	0.360	3.1
0.40	0.412	3.0

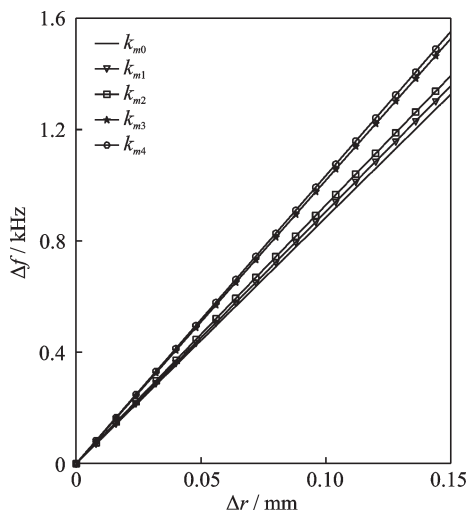


图 3 Δf_m 与 Δr 的关系

Fig.3 Relationship between Δf_m and Δr

由图 3 可知,当 Δr 不变时, m 越大则 Δf_m 也越大,即模型参数 k_m 越大,这与式(8)基本一致。

3 实验验证分析

3.1 实验平台设计

图 4 为机电阻抗实验平台,由测量设备和接地导体组成。其中,测量设备由电脑与亚德诺半导体公司的 AD5933 阻抗分析板组成,两者之间由 USB 通信,上位机软件控制 AD5933 开发板产生激励电压,驱动机电阻抗系统产生振动,并采集机电阻抗系统的电流来计算获得机电系统总阻抗实部。接地导体是碳素钢材质,长度为 500 mm、半径为 4 mm,其顶端粘贴 1 片 PZT,形成非对称传感器布置。

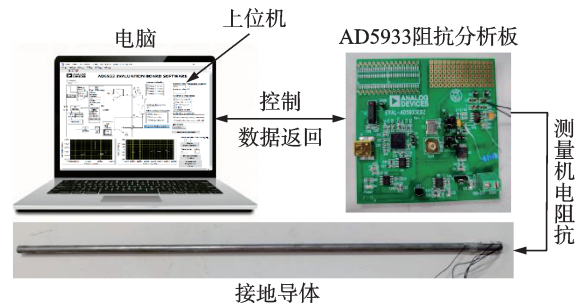


图 4 机电阻抗实验平台

Fig.4 Electromechanical impedance experimental platform

为了得到不同 Δr 的接地导体,将接地导体放置在装满土壤模拟溶液的亚克力管中,直流电源正极与接地导体相连,负极与溶液中的铜条相连,通过直流电源施加电流来对接地导体进行电化学腐蚀。土壤模拟溶液浓度如下: NaHCO_3 为 0.48 g/L; KCl 为 0.12 g/L; CaCl_2 为 0.14 g/L; MgSO_4 为 0.13g/L。NS4 溶液中还添加了少量的 NaCl 来改善导电性。由式(1)、式(2)可得直流电源加载电流大小 I 、时间 t 与腐蚀参数 Δr 的对应关系。当加载电流为 1.6 A、加载时间 $t=1.5, 3.0, 4.5, 6.0, 7.5, 9.0$ h 后,接地导体 $\Delta r=0.025, 0.05, 0.075, 0.1, 0.125, 0.15$ mm,加上 $\Delta r=0$ 的情况,接地导体共有 7 种腐蚀状态 $\Delta r=0, 0.025, 0.05, 0.075, 0.1, 0.125, 0.15$ mm。通过在自由边界下测量该系统机电阻抗实部^[14],来估计模型参数 k_m 。

3.2 自由边界条件的实验分析

为了更好地展示导体共振频率与机电总阻抗实部的关系,选择 $\Delta r=0, 0.025, 0.05, 0.075, 0.1, 0.125, 0.15$ mm,不同频率的机电阻抗如图 5 所示。由图可见,在不同 Δr 下,共振频率 f_m 出现了明显的变化。 $\Delta r=0$ 时, $f_{0,m0}=51.61$ kHz, $f_{0,m1}=54.34$ kHz, $f_{0,m2}=57.13$ kHz, $f_{0,m3}=59.95$ kHz, $f_{0,m4}=62.80$ kHz;

当 $\Delta r = 0.05$ mm 时, $f_{0.05,m0} = 51.13$ kHz, $f_{0.05,m1} = 53.86$ kHz, $f_{0.05,m2} = 56.62$ kHz, $f_{0.05,m3} = 59.41$ kHz, $f_{0.05,m4} = 62.32$ kHz; $\Delta r = 0.1$ mm 时, $f_{0.1,m0} = 50.68$ kHz, $f_{0.1,m1} = 53.41$ kHz, $f_{0.1,m2} = 56.14$ kHz, $f_{0.1,m3} = 58.93$ kHz, $f_{0.1,m4} = 61.81$ kHz; $\Delta r = 0.15$ mm 时, $f_{0.15,m0} = 50.23$ kHz, $f_{0.15,m1} = 52.93$ kHz, $f_{0.15,m2} = 55.69$ kHz, $f_{0.15,m3} = 58.42$ kHz, $f_{0.15,m4} = 61.21$ kHz。

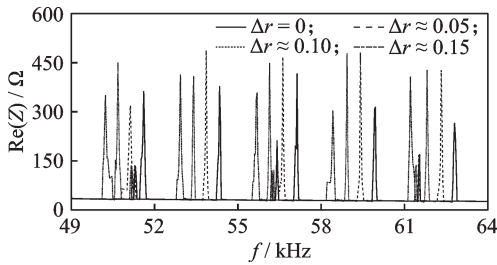


图5 不同频率的机电阻抗

Fig.5 Electromechanical impedance with frequency

当 $\Delta r = 0, 0.025, 0.05, 0.075, 0.1, 0.125, 0.15$ mm, 实验中测量获得35个各阶共振频率数据,利用最小二乘估计线性参数 k_m 。 $i = 0, 1, 2, 3, 4$ 时,可得 k_{mi} 分别为 9.154、9.394、9.634、10.35 和 10.70,对应最小二乘法的估计可信度分别为 0.9957、0.9972、0.9952、0.9976 和 0.9952,均大于 0.99。相较于有限元仿真所得到的 k_{mi} 值,5阶相对误差分别为 3.5%、3.8%、3.7%、1.7% 和 3.4%,均在 4% 范围内。

f_m 与 Δr 线性模型如图 6 所示。其中:实线为实验数据所得到的腐蚀模型 $f_{\Delta,mi} = f_{0,mi} - k_{mi}\Delta r$;星号为实验数据;虚线为有限元数据所得到的腐蚀模型;圆点为有限元数据。由图可见,实线与虚线重合性较好,说明 2 种腐蚀模型具有较好的一致性。实验与仿真结果表明,所建立的接地导体腐蚀程度与共振频率的关联模型及其量化关系可用来准确评估接地导体的腐蚀程度。

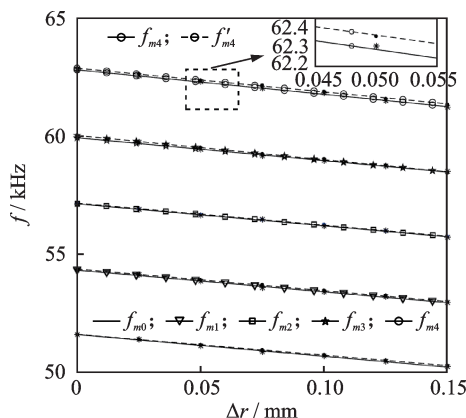


图6 f_m 与 Δr 线性模型

Fig.6 Linear model between f_m and Δr

为了分析不同共振阶数 m 对 k_m 的影响,由图 7 所示的 Δf_m 与 Δr 线性关系图可知, k_m 随着 m 的增大而增大,这与式(8)和仿真结果一致。

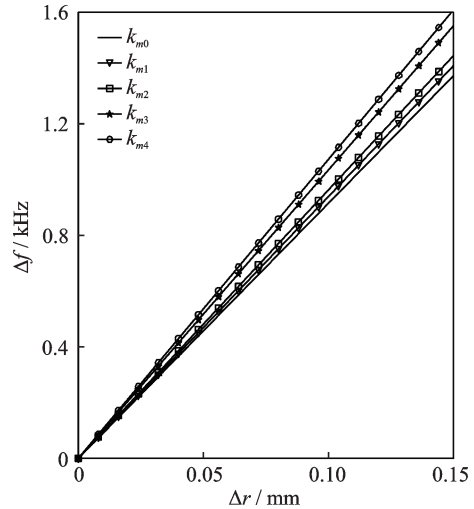


图7 Δf_m 与 Δr 线性关系图

Fig.7 Linear relationship between Δf_m and Δr

3.3 土壤边界的实验分析

在实际工况中,土壤与接地导体之间有阻尼作用,会改变接地导体的机械阻抗,影响系统的机电阻抗。因此,需要对系统机电阻抗的土壤边界条件进行测量,以验证在自由边界条件下所建立的模型是可信的。自由状态与埋置土壤的机电阻抗如图 8 所示。土壤对系统的机电阻抗产生了一定的影响,主要体现在峰值出现了小幅减小,但其共振频率 f_m 未发生偏移,这是因为土壤与机电阻抗系统之间存在的阻尼较小,阻尼作用对机电阻抗系统共振频率产生的偏移 f_m 小于测量的扫频步长 30 Hz,共振频率 f_m 不发生偏移。因此,所提出的方法也能评估埋置土壤中的接地导体的腐蚀程度。

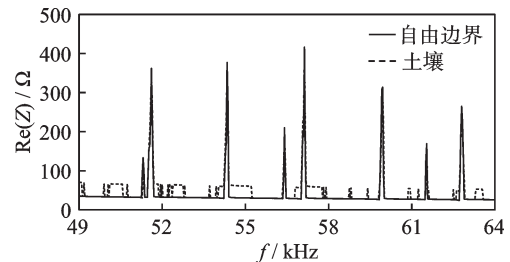


图8 自由状态与埋置土壤的机电阻抗

Fig.8 Electromechanical impedance between free and soil

4 结束语

为了解决接地导体腐蚀难以检测的问题,建立

了一种非对称传感器布置机电阻抗的共振频率 f_m 与接地导体腐蚀模型,利用有限元仿真数据,在最小二乘法误差规则下求解腐蚀模型的参数 k_m 。通过导体腐蚀实验,验证了所提出的非对称机电阻抗检测腐蚀方法的准确性。

参 考 文 献

- [1] ZHANG C, LIAO Y X, GAO X, et al. Research advances of Soil corrosion of grounding grids[J]. *Micromachines*, 2021, 12(5): 513.
- [2] WU X A, LI L X, ZHENG Y H, et al. Research on corrosion diagnostic model of grounding grid based on Tellegen's theorem[J]. *Applied Mechanics and Materials*, 2014, 672: 783-786.
- [3] LU C J, LI F, LIU Z X, et al. Location and corrosion detection of tower grounding conductors based on electromagnetic measurement[J]. *Measurement*, 2022, 199: 111469.
- [4] 张赛男, 胡伟伟, 鲍娇, 等. 金属-非金属结构累积损伤概率诊断方法[J]. *振动、测试与诊断*, 2022, 42(5): 871-876.
ZHANG Sainan, HU Weiwei, BAO Qiao, et al. Diagnosis method of cumulative damage probability for metal and non-metal structure[J]. *Journal of Vibration, Measurement & Diagnosis*, 2022, 42(5): 871-876. (in Chinese)
- [5] NGUYEN T T, PHAN T, HO D D, et al. Deep learning-based autonomous damage-sensitive feature extraction for impedance-based prestress monitoring[J]. *Engineering Structures*, 2022, 259: 114172.
- [6] ZUO C Y, FENG X, ZHANG Y, et al. Crack detection in pipelines using multiple electromechanical impedance sensors[J]. *Smart Materials and Structures*, 2017, 26(10): 104004.
- [7] TAMHANE D, BANERJEE S, TALLUR S. Monitoring corrosion in sacrificial anodes with pulsed eddy current and electromechanical impedance: a comparative analysis[J]. *IEEE Sensors Journal*, 2022, 22(8): 8147-8154.
- [8] AI D M, ZHU H P, LUO H, et al. An effective electromechanical impedance technique for steel structural health monitoring[J]. *Construction and Building Materials*, 2014, 73: 97-104.
- [9] LI W J, LIU T J, GAO S S, et al. An electromechanical impedance-instrumented corrosion-measuring probe[J]. *Journal of Intelligent Material Systems and Structures*, 2019, 30(14): 2135-2146.
- [10] WANG J J, WEN L J, LIU Z S, et al. Design and performance evaluation of electromechanical impedance instrumented quantitative corrosion measuring probe based on conical rods[J]. *Smart Materials and Structures*, 2022, 31(12): 124001.
- [11] FANG Z. A review of non-axisymmetric guided waves and their corresponding transducers for defect detection in circular tube structures[J]. *Smart Materials and Structures*, 2023, 32(6): 063001.
- [12] HUA W, SUN H, HOU Z, et al. Boosting large-current - density water oxidation activity and stability by phytic acid-assisted rapid electrochemical corrosion[J]. *Journal of Colloid and Interface Science*, 2023, 633: 24-31.
- [13] AI D M, DU L X, LI H D, et al. Corrosion damage identification for reinforced concrete beam using embedded piezoelectric transducer: numerical simulation [J]. *Measurement*, 2022, 192: 110925.
- [14] ZHU J J, QING X L, LIU X, et al. Electromechanical impedance-based damage localization with novel signatures extraction methodology and modified probability-weighted algorithm[J]. *Mechanical Systems and Signal Processing*, 2021, 146: 107001.
- [15] 揭小落, 肖黎, 屈文忠. 载荷影响下的机电阻抗协整结构损伤识别方法[J]. *振动、测试与诊断*, 2020, 40(3): 526-534.
JIE Xiaoluo, XIAO Li, QU Wenzhong. Structural damage identification under load based on electromechanical impedance con-integration[J]. *Journal of Vibration, Measurement & Diagnosis*, 2020, 40(3): 526-534. (in Chinese)



第一作者简介:黄宴委,男,1976年3月生,博士、教授。主要研究方向为智能检测。

E-mail: sjtu_huanghao@fzu.edu.cn

通信作者简介:方舟,男,1988年7月生,博士、副教授。主要研究方向为超声导波无损检测。

E-mail: fz@fzu.edu.cn

of the stable regions of the system is analyzed, and the appropriate disengaging speed range of the damping structure is obtained. Finally, the effect of the damping structure for suppressing transient suppression of the washer is validated through experiments, and the appropriate disengaging speed of the structure is analyzed. The results show that the planar damping structure can suppress transient vibrations effectively with little influence on other dynamic characteristics of the washer.

Keywords washing machine; transient vibration; vibration suppression; variable damping structure; stability analysis

Research on Noise Reduction of Inertial Navigation Heterogeneous Signals Based on Noise-Sensitive Prior and Improved VMD

LIU Yu^{1,2}, CHEN Long¹, TAO Lei², WANG Hongwei^{1,2}, HUANG Qingxue^{1,2}

(1. College of Mechanical Engineering, Taiyuan University of Technology Taiyuan, 030024, China)

(2. State Key Laboratory of Intelligent Mining Equipment Technology Taiyuan, 030032, China)

Abstract Aiming at the multi-source noise of inertial navigation in the attitude estimation of coal mine bolting jumbo, a noise reduction method of inertial navigation heterogeneous signal is proposed based on noise sensitive prior and improved variational mode decomposition (VMD), which avoids the over-decomposition and under-decomposition problems caused by the parameter fixation. Firstly, the noise sensitivity difference of the heterogeneous signals (acceleration and angular velocity) of coal mine bolting jumbo is investigated by using the variation of the signal characteristics in the time and frequency domains. Secondly, according to the noise-sensitive characteristics, the dual decomposition layer and energy fluctuation model are constructed, so that the decomposition parameters have the ability of adaptive optimization and the synchronous optimal decomposition of the inertial-guide heterogeneous signals is realized. Based on the Pearson correlation coefficient (PCC), the modal component screening parameter, correlation coefficient P , is designed to consider the noise sensitivity difference, to achieve screening practical modal components and simultaneous noise reduction of heterogeneous signals. Finally, the proposed method is compared with the noise reduction results of complementary ensemble empirical mode decomposition (CEEMD) and improved complete ensemble empirical mode decomposition with adaptive noise (ICEEMDAN). The results show that the method proposed in this paper considers the noise sensitivity differences of heterogeneous signals, thereby improving the signal-to-noise ratio of inertial measurement and enhancing the attitude initialization accuracy of bolting jumbo. The pitch error is reduced by 81.818%, and the yaw error is reduced by 87.958%, which lays a good foundation for accurate roadway support.

Keywords variational mode decomposition; noise reduction; inertial navigation heterogeneous signal; bolting jumbo

Corrosion Evaluation Technology by Electromechanical Impedance for Grounding Conductors

HUANG Yanwei, CHEN Yaojie, ZHANG Haojun, FANG Zhou

(Department of Automation, Fuzhou University Fuzhou, 350116, China)

Abstract A novel approach based on electromechanical impedance is proposed to evaluate the corrosion degree

for grounding conductors, which are difficult to simply detect and evaluate for traditional methods. Firstly, according to the electrochemical corrosion model of metals, the grounding conductor parametric corrosion model is established by importing the change of grounding conductor radius as corrosion parameter. Secondly, the corrosion model between an electromechanical impedance resonance frequency and corrosion parameter is established with the analysis of system electromechanical impedance and conductor mechanical admittance. Then, the resonance frequency and corrosion parameter signal of grounding conductors are obtained via finite element simulation method, while the coefficient of the corrosion model is obtained by the least square method. The results show that the electromechanical impedance detected by asymmetrical sensor layout can reflect variations of the corrosion parameter more clearly than that by symmetrical sensor layout. Linear model by finite element simulation and the least square method can predict the corrosion parameter. Moreover, the high consistency between the datum predicted by the linear model and the experimental datum, indicates the linear model is very accurate and can be used to detect the conductor corrosion in field applications.

Keywords grounding conductor; parametric corrosion model; electromechanical impedance; finite element simulation

Study on the Characteristics of Fluid-Structure Interaction Wind Effects in Super High-Rise Buildings Subject to Various Inflow Conditions

LU Chunling^{1,2,3}, WU Min¹, CHEN Xudong¹, WANG Qiang^{1,2,3}

(1. Guangxi Key Laboratory of Green Building Materials and Construction Industrialization Guilin, 541004, China)

(2. College of Civil Engineering, Guilin University of Technology Guilin, 541004, China)

(3. Guangxi Engineering Research Center of Intelligent Structural Material Guilin, 541004, China)

Abstract To study the wind effect characteristics of super high-rise buildings in different incoming flows under the fluid-structure interaction effect, a full-scale numerical wind tunnel simulation of Pingan Financial Building in Shenzhen is carried out using the detached eddy simulation (DES), established the aeroelastic model. A new turbulent fluctuating flow field generation method named the discretizing and synthesizing random flow generator (DSRFG) is used to simulate the turbulent flows of the atmospheric boundary layer and the uniform flows. The wind pressure and wind-induced response results of the model are obtained. The calculated results are compared with the corresponding data from wind tunnel tests and field measurements to verify the accuracy of the numerical simulation. The analysis shows that the wind pressure of the building under turbulent incoming flow obtained from the DES is consistent with the distribution trend of wind tunnel test and field measurement results. The distribution of the mean wind pressure coefficient of the building under both conditions is similar, and the fluctuating wind pressure coefficient on the windward side under turbulent incoming flow is larger than that under uniform incoming flow. In addition, the cross-wind acceleration response is larger under turbulent incoming flow than that under uniform incoming flow, and the acceleration response power spectrum shows three peaks and the displacement response power spectrum shows two peaks under uniform incoming flow, while the turbulent incoming flow only shows a single peak. The acceleration response power spectrum shows three peaks and displacement response power spectrum shows double peaks under uniform incoming flow with only single peak under turbulent incoming flow. In the flow field, the wind velocity is more uniform in the uniform incoming flow than in the turbulent incoming flow, the wake vortex is flatter and narrower, and the overall vorticity magnitude is smaller.